Analysis of flux-integrated cross sections for quasi-elastic neutrino charged-current scattering off ^{12}C at energies available at the MiniBooNE experiment

A. V. Butkevich

Institute for Nuclear Research, Russian Academy of Sciences, 60th October Anniversary Prospect 7A, Moscow 117312, Russia

(Received 15 June 2010; published 11 November 2010)

Flux-averaged and flux-integrated cross sections for quasi-elastic neutrino charged-current scattering on nuclei are analyzed. It is shown that the flux-integrated differential cross sections are less dependent on nuclear models than the flux-averaged ones. We calculate these cross sections using the relativistic distorted-wave impulse approximation and relativistic Fermi gas model with the Booster Neutrino Beamline flux and compare the results with the recent MiniBooNE experimental data. Within these models an axial mass M_A is extracted from a fit of the measured $d\sigma/dQ^2$ cross section. The extracted value of $M_A = 1.37 \pm 0.05$ GeV/c^2 is consistent with the MiniBooNE result. While the measured and calculated double differential cross sections $d\sigma/dTd\cos\theta$ generally agree, the Fermi gas model predictions are typically lower than data at low muon energies and scattering angles.

DOI: 10.1103/PhysRevC.82.055501 PACS number(s): 25.30.Pt, 25.30.Bf, 13.15.+g

I. INTRODUCTION

The current [1–4] and planned [5] sets of accelerator-based neutrino experiments use extremely intense neutrino beamlines for precise measurements of the observed neutrino mass splitting and mixing angles and a detailed experimental study of the neutrino mixing matrix. The intense beamlines used in these experiments will greatly improve their statistical precision.

In this situation, the statistical uncertainties should be negligible when compared to systematic errors. Poorly measured neutrino-nucleus cross sections are a leading source of systematic errors. The neutrino beams of high intensity cover the few-GeV energy range, where the dominant contribution to the νA cross section comes from charged-current quasi-elastic (CCQE) scattering and resonance production processes. In the long-baseline neutrino oscillation experiments, near and far detectors are used to normalize the neutrino flux at production and to search for the neutrino oscillation effects. While many unknown quantities are eliminated in these experiments by considering ratios of far to near events, the cancellation is not complete due to differences in neutrino flux and backgrounds in the near and far detectors. Thus, to permit precision oscillation measurements, it is important to have an accurate characterization of the CCQE differential cross sections over a wide span of neutrino energies.

The current data on CCQE scattering come from a variety of experiments operating at differing energies and with different nuclei. The existing data on (anti)neutrino CCQE scattering come mostly from bubble chamber experiments, which suffer from poor statistics. In general, the experimental execution and data interpretation are nontrivial for several reasons. Neutrino beams typically span a wide energy range. The neutrino flux itself is often poorly known, and a background from resonance processes is frequently significant and difficult to separate from the CCQE signal. Therefore, the total QE cross sections measured in different experiments have typical uncertainties of 20–40%. Even within such large uncertainties some results contradict each other. The difference between the total quasi-elastic cross sections, calculated within the framework of various models [6–19] is lower than the spread in the data.

More information about the neutrino-nuclear CCQE interaction can be obtained from the analysis of CCQE event distributions and $d\sigma/dQ^2$ differential cross sections as functions of Q^2 (squared four-momentum transfer) [20]. The shape of these distributions is sensitive to the Q^2 dependence of two vector $F_{1,2}(Q^2)$, one axial-vector $F_A(Q^2)$ form factors, and nuclear effects. The vector form factors are well known from electron scattering. For the axial-vector form factor, the dipole parametrization with one free parameter M_A (axial mass) is mainly used. This parameter controls the Q^2 dependence of $F_A(Q^2)$ and, ultimately, the normalization of the predicted cross sections. The dipole parametrization has no strict theoretical basis and the choice of this parametrization is borrowed from the traditional parametrizations of the vector form factors. To describe the nuclear effects, neutrino CCQE models typically employ a relativistic Fermi gas model (RFGM) [6] in which the nucleons have a flat nucleon momentum distribution up to the some Fermi momentum p_F and nuclear binding energy ϵ_b. The experimental values of M_A are extracted from (anti)neutrino CCQE scattering data (i.e., from the analysis of the shape of the Q^2 distributions and from the direct measurements of the total cross sections). They show a very wide spread from roughly 0.7 to 1.2 GeV and the resulting world average is $M_A = 1.026 \pm 0.021$ GeV [21].

Several experiments recently reported new results on CCQE scattering from high-statistics data samples with intense, well-understood neutrino beams. The Neutrino Oscillation Magnetic Detector (NOMAD) experiment [22] observed an M_A value and cross section (from data taken on carbon) consistent with the prior world average. However, the data of Refs. [1,23–26] (preliminary result), collected on carbon, oxygen, and iron targets, indicated a somewhat larger value for $M_A = 1.19$–1.37 GeV/c^2. In these experiments the shape of the Q^2 distribution was analyzed.

These data show a disagreement with the RFGM predictions. The data samples exhibit a deficit in the region of low $Q^2 \leqslant 0.2$ (GeV/c)^2 (the so-called low-Q^2 problem). It is known from the comparison with the low-energy QE electron-nucleus scattering data that the RFGM description of this region is not accurate enough [27]. There is a data

excess in the region of high-Q^2 and the value of M_A, obtained from a fit to the measured data, is higher than the results of previous experiments. The collection of existing results remains puzzling. The next experiments, Main Injector Experiment Neutrino-A (MINERvA) [28] and MicroBooNE [29] as well as the T2K [3] and NOvA [5] near detectors will be able to make more precise measurements of the CCQE cross sections in a wide range of energies and for various nuclear targets.

The uncertainties in the theoretical description of the quasi-elastic neutrino-nucleus scattering can be considerably reduced if new model-independent absolute differential cross sections can be provided. The first measurement of the flux-integrated double-differential cross section (in muon energy and angle) for CCQE scattering on carbon has been produced by the MiniBooNE experiment [30]. This cross section contains the most complete and model-independent information that is available for the CCQE process.

The aim of this work is to test the RFGM and relativistic distorted-wave impulse approximation (RDWIA) predictions against the MiniBooNE data [30]. In the framework of these approaches we extract the values of axial mass from the measured flux-integrated $d\sigma/dQ^2$ cross section. Then, using these extracted values of M_A, we calculate the flux-integrated differential and flux-unfolded total cross sections and compare the results with data.

The outline of this article is as follows. In Sec. II we present briefly the RDWIA model and discuss the flux-averaged and flux-integrated differential cross sections. The results are presented in Sec. III. Our conclusions are summarized in Sec. IV.

II. MODEL, FLUX-AVERAGED, AND FLUX-INTEGRATED DIFFERENTIAL CROSS SECTIONS

We consider neutrino CCQE exclusive

$$\nu(k_i) + A(p_A) \to \mu(k_f) + N(p_x) + B(p_B), \tag{1}$$

and inclusive

$$\nu(k_i) + A(p_A) \to \mu(k_f) + X, \tag{2}$$

scattering off nuclei in the one-W-boson exchange approximation. Here $k_i = (\varepsilon_i, \boldsymbol{k}_i)$ and $k_f = (\varepsilon_f, \boldsymbol{k}_f)$ are the initial and final lepton momenta, $p_A = (\varepsilon_A, \boldsymbol{p}_A)$ and $p_B = (\varepsilon_B, \boldsymbol{p}_B)$ are the initial and final target momenta, $p_x = (\varepsilon_x, \boldsymbol{p}_x)$ is the ejectile nucleon momentum, $q = (\omega, \boldsymbol{q})$ is the momentum transfer carried by the virtual W boson, and $Q^2 = -q^2 = \boldsymbol{q}^2 - \omega^2$ is the W-boson virtuality.

A. Model

The formalism of CCQE exclusive and inclusive reactions is described in Ref. [17]. All the nuclear structure information and final state interaction effects (FSI) are contained in the weak CC nuclear tensors $W_{\mu\nu}$, which are given by the bilinear product of the transition matrix elements of the nuclear CC operator J_μ between the initial nucleus state $|A\rangle$ and the final state $|B_f\rangle$ as

$$W_{\mu\nu} = \sum_f \langle B_f, p_x | J_\mu | A \rangle \langle A | J_\nu^\dagger | B_f, p_x \rangle, \tag{3}$$

where the sum is taken over undetected states.

We describe CCQE neutrino-nuclear scattering in the impulse approximation (IA), assuming that the incoming neutrino interacts with only one nucleon, which is subsequently emitted, while the remaining (A-1) nucleons in the target are spectators. When the nuclear current is written as the sum of single-nucleon currents, the nuclear matrix element in Eq. (3) takes the form

$$\langle p, B | J^\mu | A \rangle = \int d^3r \exp(i\boldsymbol{t}\cdot\mathbf{r}) \overline{\Psi}^{(-)}(\boldsymbol{p}, \mathbf{r}) \Gamma^\mu \Phi(\mathbf{r}), \tag{4}$$

where Γ^μ is the vertex function, $\boldsymbol{t} = \varepsilon_B \boldsymbol{q}/W$ is the recoil-corrected momentum transfer, $W = \sqrt{(m_A + \omega)^2 - \boldsymbol{q}^2}$ is the invariant mass, Φ and $\Psi^{(-)}$ are the relativistic bound-state and outgoing wave functions.

The single-nucleon charged current has $V-A$ structure $J^\mu = J_V^\mu + J_A^\mu$. For a free-nucleon vertex function $\Gamma^\mu = \Gamma_V^\mu + \Gamma_A^\mu$ we use the vector current vertex function $\Gamma_V^\mu = F_V(Q^2)\gamma^\mu + i\sigma^{\mu\nu}q_\nu F_M(Q^2)/2m$, where $\sigma^{\mu\nu} = i[\gamma^\mu, \gamma^\nu]/2$, and F_V and F_M are the weak vector form factors. They are related to the corresponding electromagnetic form factors for protons and neutrons by the hypothesis of the conserved vector current. We use the approximation of Ref. [31] for the nucleon form factors. Because the bound nucleons are the off-shell we employ the de Forest prescription [32] and Coulomb gauge for the off-shell vector current vertex Γ_V^μ. The vector-axial and pseudoscalar form factors are parametrized as a dipole with the axial-vector mass, which controls the Q^2 dependence of F_A, and ultimately, the normalization of the predicted cross section.

According to the JLab data [33,34] the occupancy of the independent particle shell-model (IPSM) orbitals of ^{12}C equals on average 89%. In this work we assume that the missing strength (11%) can be attributed to the short-range nucleon-nucleon (NN) correlations in the ground state, leading to the appearance of the high-momentum (HM) and high-energy component in the nucleon distribution in the target. To estimate this effect in the inclusive cross sections, we consider a phenomenological model that incorporates both the single-particle nature of the nucleon spectrum at low energy (IPSM orbitals) and the high-energy and high-momentum components due to NN correlations.

In the IPSM, the relativistic wave functions of the bound nucleon states Φ are obtained as the self-consistent (Hartree-Bogoliubov) solutions of a Dirac equation, derived within a relativistic mean-field approach, from a Lagrangian containing σ, ω, and ρ mesons (the σ-ω model) [35]. We use the nucleon bound-state functions calculated for carbon by the TIMORA code [36] with the normalization factors $S(\alpha)$ relative to the full occupancy of the IPSM orbitals of ^{12}C: $S(1p_{3/2}) = 84\%$, $S(1s_{1/2}) = 100\%$, and an average factor of about 89%. These estimations of the depletion of hole states follow from the RDWIA analysis of ^{12}C$(e,e'p)$ for $Q^2 < 2$ (GeV/c)^2 [34] and are consistent with a direct measurement of the spectral function using ^{12}C$(e,e'p)$ in parallel kinematics [37], which

observed approximately 0.6 protons in a region attributable to a single-nucleon knockout from a correlated cluster.

For the outgoing nucleon, the simplest choice is to use plane-wave function Ψ, that is, no interactions are considered between the ejected nucleon N and the residual nucleus B . For a more realistic description, FSI effects should be taken into account. In the RDWIA the distorted wave function Ψ is evaluated as a solution of a Dirac equation containing a phenomenological relativistic optical potential. The channel coupling in the FSI [38] of the $N + B$ system is taken into account. The relativistic optical potential consists of a real part which describes the rescattering of the ejected nucleon and an imaginary part that accounts for the absorption of it into unobserved channels.

Using the direct Pauli reduction method, the system of two coupled first-order radial Dirac equations can be reduced to a single second-order Schrödinger-like equation for the upper component of the Dirac wave function Ψ. We use the LEA program [39] for the numerical calculation of the distorted wave functions with the EDAD1 parametrization [40] of the relativistic optical potential for carbon. This code, initially designed for computing exclusive proton-nucleus and electron-nucleus scattering, was successfully tested against $A(e,e'p)$ data [33,41] and we adopted this program for neutrino reactions.

A complex optical potential with a nonzero imaginary part generally produces an absorption of the flux. For the exclusive $A(l,l'N)$ channel this reflects the coupling between different open reaction channels. However, for the inclusive reaction, the total flux must be conserved. In Refs. [9,42], it was shown that the inclusive CCQE neutrino cross section of the exclusive channel $A(l,l'N)$ calculated with only the real part of the optical potential is almost identical when calculated via the Green's function approach [9,43] in which the FSI effects on inclusive reaction $A(l,l'X)$ are treated by means of a complex potential and the total flux is conserved. We calculate the inclusive and total cross sections with the EDAD1 relativistic optical potential in which only the real part is included.

The inclusive cross sections with the FSI effects in the presence of the short-range NN correlations were calculated using the method proposed in Ref. [17]. In this approach the contribution of the NN correlated pairs is evaluated in the plane-wave impulse approximation (PWIA) model. We use the general expression for the high-momentum and high-energy part of the spectral function from Ref. [44] with the parametrization for the nucleon high-momentum distribution from Ref. [45], which was renormalized to a value of 11%. The FSI effects for the high-momentum component are estimated by scaling the PWIA cross section with the $\Lambda(\varepsilon_f \Omega_f)$ function determined in Ref. [17].

B. Flux-averaged and flux-integrated differential cross sections

In neutrino experiments the differential cross sections of CCQE neutrino-nucleus scattering are measured within rather wide ranges of the (anti)neutrino energy spectrum. Therefore flux-averaged and flux-integrated differential cross sections can be extracted.

Because the ν_μ mode of beams incorporates ν_μ and $\bar{\nu}_\mu$ spectra, the flux-averaged double differential cross section $d^2\sigma/dT\,d\cos\theta$ in muon kinetic energy T and muon scattering angle θ is the sum of neutrino and antineutrino cross sections

$$\left\langle \frac{d^2\sigma}{dT\,d\cos\theta} \right\rangle = \left\langle \frac{d^2\sigma^{\nu}}{dT\,d\cos\theta} \right\rangle + \left\langle \frac{d^2\sigma^{\bar{\nu}}}{dT\,d\cos\theta} \right\rangle, \tag{5}$$

where

$$\left\langle \frac{d^2\sigma^{\nu,\bar{\nu}}}{dT\,d\cos\theta}(T,\cos\theta) \right\rangle = \int_{\varepsilon_1}^{\varepsilon_2} W_{\nu,\bar{\nu}}(T,\cos\theta,\varepsilon_i) \frac{d^2\sigma^{\nu,\bar{\nu}}}{dT\,d\cos\theta}(T,\cos\theta,\varepsilon_i)\,d\varepsilon_i, \tag{6}$$

and $W_{\nu,\bar{\nu}}$ are weight functions. The normalization of these functions is given by

$$\int_{\varepsilon_1}^{\varepsilon_2} [W_{\nu}(T,\cos\theta,\varepsilon_i) + W_{\bar{\nu}}(T,\cos\theta,\varepsilon_i)]d\varepsilon_i = 1. \tag{7}$$

The weight functions are defined as

$$W_{\nu,\bar{\nu}}(T,\cos\theta,\varepsilon_i) = I_{\nu,\bar{\nu}}(\varepsilon_i)/\Phi(T,\cos\theta), \tag{8}$$

where $I_{\nu,\bar{\nu}}$ is the neutrino (antineutrino) spectrum in the ν mode of the flux and

$$\Phi(T,\cos\theta) = \int_{\varepsilon_1}^{\varepsilon_2} [I_{\nu}(\varepsilon_i) + I_{\bar{\nu}}(\varepsilon)]d\varepsilon_i, \tag{9}$$

are the neutrino and antineutrino fluxes that give the contribution to the measured double differential cross section at fixed values of $(T,\cos\theta)$. This flux depends on $(T,\cos\theta)$ due to the limits of integration in Eqs. (6), (7), and (9), which are functions of $(T,\cos\theta)$ [i.e., $\varepsilon_i = \varepsilon_{\min}(T,\cos\theta)$ and $\varepsilon_2 = \varepsilon_{\max}(T,\cos\theta)$]. In Fig. 1 the double differential cross sections, calculated within the RDWIA and RFGM (with the Fermi momentum $p_F = 221$ MeV/c and a binding energy $\epsilon_b = 25$ MeV for carbon), are shown as functions of neutrino energy. Apparently the ranges $[\varepsilon_{\max}(T,\cos\theta) - \varepsilon_{\min}(T,\cos\theta)]$, where $d\sigma^2/dT\,d\cos\theta$ is not equal to zero, are different in the RDWIA and RFGM. Therefore, the value of $\Phi(T,\cos\theta)$ is model dependent and ultimately the weight functions and the cross section $\langle d^2\sigma/dT\,d\cos\theta\rangle$ depend on nuclear models as well. Note that the flux $\Phi(T,\cos\theta)$ should be used to extract the measured flux-averaged cross section in the i,j bins of $(T,\cos\theta)$ variables (for example, see Eq. (3) in Ref. [30]).

Similarly, the flux-averaged $d\sigma/dQ^2$ cross section can be written as the sum

$$\left\langle \frac{d\sigma}{dQ^2} \right\rangle = \left\langle \frac{d\sigma^{\nu}}{dQ^2} \right\rangle + \left\langle \frac{d\sigma^{\bar{\nu}}}{dQ^2} \right\rangle, \tag{10}$$

where

$$\left\langle \frac{d\sigma^{\nu,\bar{\nu}}}{dQ^2}(Q^2,T_{\rm th}) \right\rangle = \int_{\varepsilon_1}^{\varepsilon_2} W_{\nu,\bar{\nu}}(Q^2,\varepsilon_i) \frac{d\sigma^{\nu,\bar{\nu}}}{dQ^2}(Q^2,T_{\rm th},\varepsilon_i)\,d\varepsilon_i, \tag{11}$$

and $T_{\rm th}$ is the muon threshold energy after all cuts for the CCQE events selection.

The weight functions in Eq. (11) are defined as follows:

$$W_{\nu,\bar{\nu}}(Q^2,\varepsilon_i) = I_{\nu,\bar{\nu}}(\varepsilon_i)/\Phi(Q^2), \tag{12}$$

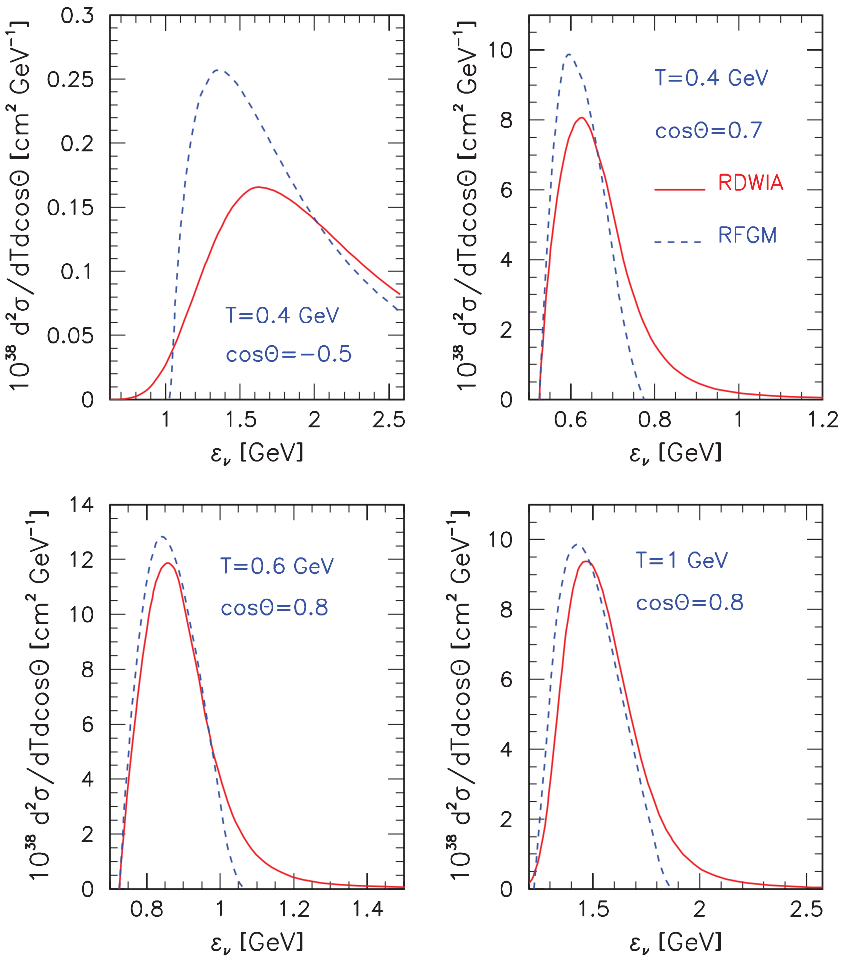

FIG. 1. (Color online) Double differential cross sections vs. the neutrino energy calculated in the RDWIA (solid line) and RFGM (dashed line) approaches for the four values of $(T, \cos\theta)$: (0.4 GeV, −0.5), (0.4 GeV, 0.7), (0.6 GeV, 0.8), and (1 GeV, 0.8).

where

$$\Phi(Q^2) = \int_{\varepsilon_1}^{\varepsilon_2} [I_\nu(\varepsilon_i) + I_{\bar\nu}(\varepsilon)] d\varepsilon_i, \tag{13}$$

are the neutrino and antineutrino fluxes that give the contribution to the measured cross section at the fixed value of Q^2. The flux is a function of Q^2 because $\varepsilon_1 = \varepsilon_{\min}(Q^2)$ and $\varepsilon_2 = \varepsilon_{\max}$, where $\varepsilon_{\max}$ is the maximum energy in the (anti)neutrino spectrum. The limit $\varepsilon_{\min}(Q^2)$ and ultimately the flux $\Phi(Q^2)$ depend on the nuclear model. As a result, the extracted flux-averaged cross section $\langle d\sigma/dQ^2\rangle$ is also model dependent.

In Eq. (11) the cross section $d\sigma/dQ^2$ is defined as

$$\frac{d\sigma}{dQ^2}(Q^2, T_{\rm th}, \varepsilon_i) = \int_{\omega_{\min}}^{\omega_{\rm cut}} \frac{d^2\sigma}{dQ^2 d\omega}(Q^2, \omega)\, d\omega, \tag{14}$$

where $\omega_{\rm cut} = \min\{\omega_{\max}(Q^2), \varepsilon_i - m_\mu - T_{\rm th}\}$, m_μ is the muon mass, and $\omega_{\max}(Q^2)$ and $\omega_{\min}(Q^2)$ are the limits of the kinematic allowed ω range at the fixed value of Q^2. If $T_{\rm th} = 0$, the upper limit $\omega_{\rm cut} = \omega_{\max}(Q^2)$. So the flux-averaged differential $\langle d\sigma^2/dT d\cos\theta\rangle$ and $\langle d\sigma/dQ^2\rangle$ cross sections are model dependent.

In Ref. [30] the differential cross sections were extracted using the flux $\Phi_{\rm BNB}$ that was determined by integration of the Booster Neutrino Beamline flux [46] over $0 \leqslant \varepsilon_i \leqslant 3$ GeV (i.e., $\Phi_{\rm BNB}$ is a single number, $2.90 \times 10^{11} \nu_\mu/{\rm cm}^2$). Therefore, these flux-integrated differential cross sections are not model dependent and can be written as

$$\left(\frac{d^2\sigma}{dT d\cos\theta}\right)^{\rm int} = \left(\frac{d^2\sigma^\nu}{dT d\cos\theta}\right)^{\rm int} + \left(\frac{d^2\sigma^{\bar\nu}}{dT d\cos\theta}\right)^{\rm int}, \tag{15}$$

where

$$\left(\frac{d^2\sigma^{\nu,\bar\nu}}{dT d\cos\theta}(T, \cos\theta)\right)^{\rm int} = \int_{\varepsilon_1}^{\varepsilon_2} \widetilde{W}_{\nu,\bar\nu}(\varepsilon_i) \frac{d^2\sigma^{\nu,\bar\nu}}{dT d\cos\theta}(T, \cos\theta, \varepsilon_i)\, d\varepsilon_i, \tag{16}$$

and

$$\left(\frac{d\sigma}{dQ^2}\right)^{\rm int} = \left(\frac{d\sigma^\nu}{dQ^2}\right)^{\rm int} + \left(\frac{d\sigma^{\bar\nu}}{dQ^2}\right)^{\rm int}, \tag{17}$$

where

$$\left(\frac{d\sigma^{\nu,\bar\nu}}{dQ^2}(Q^2, T_{\rm th})\right)^{\rm int} = \int_{\varepsilon_1}^{\varepsilon_2} \widetilde{W}_{\nu,\bar\nu}(\varepsilon_i) \frac{d\sigma^{\nu,\bar\nu}}{dQ^2}(Q^2, T_{\rm th}, \varepsilon_i)\, d\varepsilon_i. \tag{18}$$

The weight functions $\widetilde{W}_{\nu,\bar\nu}$ are defined as

$$\widetilde{W}_{\nu,\bar\nu}(\varepsilon_i) = I_{\nu,\bar\nu}(\varepsilon_i)/\Phi_{\rm BNB}, \tag{19}$$

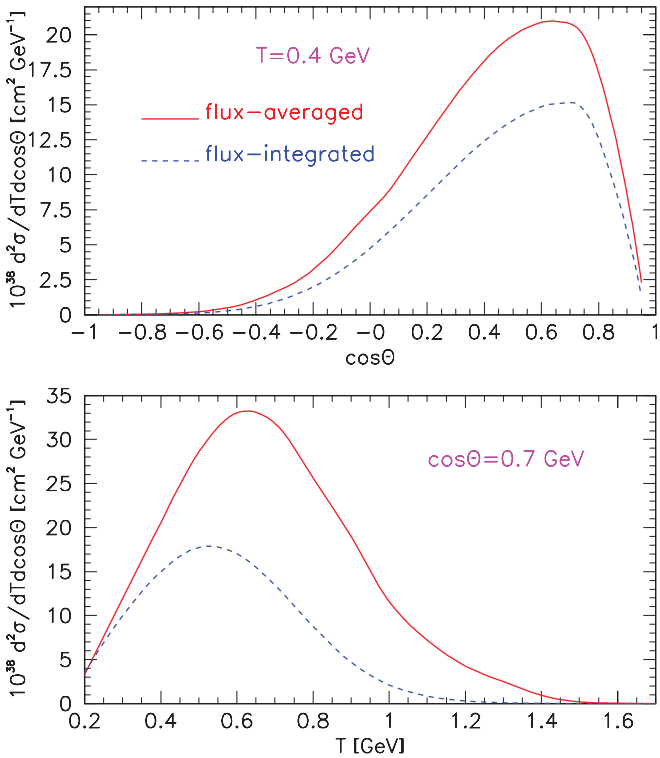

FIG. 2. (Color online) Flux-averaged (solid line) and flux-integrated (dashed line) double differential cross sections versus $\cos\theta$ for $T = 0.4$ GeV (upper panel) and versus T for $\cos\theta = 0.7$ (lower panel) calculated in the RDWA approach for the ν mode of the BNB flux.

and

$$\int_{\varepsilon_1}^{\varepsilon_2} [\widetilde{W}_{\nu}(\varepsilon_i) + \widetilde{W}_{\bar{\nu}}(\varepsilon_i)] d\varepsilon_i \leqslant 1. \tag{20}$$

because $\Phi_{\rm BNB} \geqslant \Phi(T, \cos\theta)$ and $\Phi_{\rm BNB} \geqslant \Phi(Q^2)$. These functions depend only on (anti)neutrino energy and are model independent. As an example, on Fig. 2 the flux-averaged and flux-integrated double differential cross sections calculated within the RDWIA model for the ν mode of the BNB flux are compared. The flux-averaged cross sections are higher than the flux-integrated ones. This is because the normalization of $\widetilde{W}_{\nu,\bar{\nu}}$ [Eq.(20)] is less than unity. From the practical point of view, the extracted flux-integrated differential cross sections are more useful than the flux-averaged ones because they feature minimal model dependence and can be used for a comparison to models of CCQE interactions on nuclei.

III. RESULTS AND ANALYSIS

A. CCQE flux-integrated $d\sigma/dQ^2$ differential cross section

New data for the Q^2 distribution of CCQE events measured in the MiniBooNE experiment were presented in Refs. [30,47]. The measured, instead of calculated, CC one pion production (CC1π^+) background was subtracted [1]. With the measured CC1π^+ background incorporated, a "shape-only" fit to the CCQE events sample was performed to extract values for adjusted CCQE model parameters M_A and κ within the Fermi gas model. To tune this model to the low Q^2 the parameter κ was introduced [1], which reduced the phase-space volume at low-momentum transfer. Note that when $\kappa = 1$ the phase-space volume is the same as in the "standard" RFGM. This parameter controls the Q^2 distribution only in the low-Q^2 region. The shape-only fit yields the model parameters, $M_A = 1.35 \pm 0.17$ GeV/c^2 and $\kappa = 1.007 \pm 0.012$. The extracted value for M_A is approximately 30% higher than the world average.

The MiniBooNE ν_μ CC flux-integrated single differential per neutron cross section $d\sigma/dQ^2$ was extracted as a function of Q^2 in the range $0 \leqslant Q^2 \leqslant 2$ (GeV/c)^2. To extract a value for the parameter M_A we calculated this cross section with the BNB flux in the RDWIA and RFGM models using the Q^2 bins $\Delta Q^2 = Q^2_{i+1} - Q^2_i$ similar to [30]

$$\left(\frac{d\sigma}{dQ^2}\right)_i^{\rm int} = \frac{1}{\Delta Q^2} \int_{Q^2_i}^{Q^2_{i+1}} \left[\frac{d\sigma}{dQ^2}(Q^2)\right]^{\rm int} dQ^2. \tag{21}$$

Because the data include events with $T \leqslant 200$ MeV [30], we calculated $d\sigma/dQ^2$ with $T = 0$ in Eq. (14). Within the RDWIA (RFGM) model the fit to the extracted flux-integrated $d\sigma/dQ^2$ cross section with only-shape error yields the parameter $M_A = 1.37 \pm 0.05$ GeV/c^2 ($M_A = 1.36 \pm 0.05$ GeV/c^2). These values are consistent with the MiniBooNE result $M_A = 1.37 \pm 0.17$ GeV/c^2.

Figure 3 shows measured flux-integrated $d\sigma/dQ^2$ differential cross section as a function of Q^2 compared with the RDWIA ($M_A = 1.37$ GeV/c^2) and RFGM ($M_A = 1.36$ GeV/c^2) calculations. There is an overall agreement between the RDWIA result and the data across the full range of Q^2, whereas the RFGM overestimates the measured

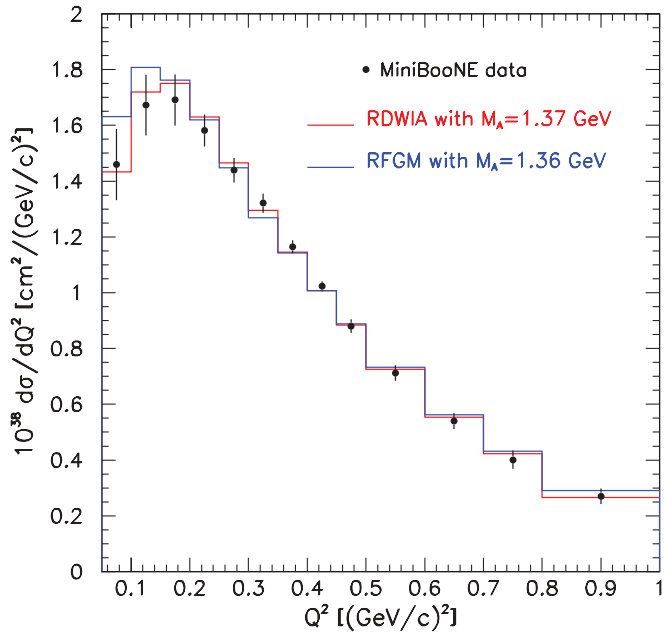

FIG. 3. (Color online) Flux-integrated $d\sigma/dQ^2$ cross section per neutron target for the ν_μ CCQE scattering. Calculations from the RDWIA with $M_A = 1.37$ GeV/c^2 and RFGM with $M_A = 1.36$ GeV/c^2. The MiniBooNE data are shown as points with the shape error only.

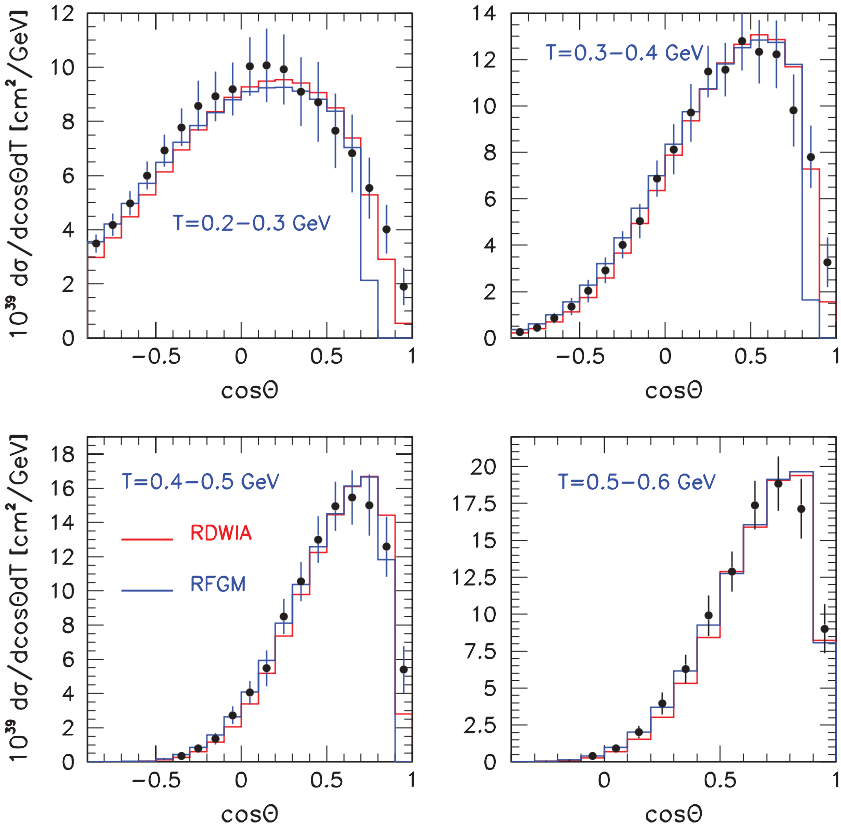

FIG. 4. (Color online) Flux-integrated $d^2\sigma/dT\,d\cos\theta$ per neutron cross section for the ν_μ CCQE process as a function of $\cos\theta$ for the four muon kinetic energy bins: T(GeV) = (0.2–0.3), (0.3–0.4), (0.4–0.5), and (0.5–0.6). As shown in the key, cross sections were calculated within the RDWIA ($M_A = 1.37$ GeV/c^2) and RFGM ($M_A = 1.36$ GeV/c^2). The MiniBooNE data are shown as points with the shape error only.

differential cross section at $Q^2 \leqslant 0.2$ (GeV/c)^2. At higher Q^2 a good match between the RFGM calculated and measured cross sections is observed. Thus, the so-called low-Q^2 problem is successfully solved in the distorted wave approach.

B. CCQE flux-integrated double differential cross section

The flux-integrated double differential per neutron cross section $d^2\sigma/dT\,d\cos\theta$ for the ν_μ CCQE process was extracted in Ref. [30] for the kinematic range $-1 < \cos\theta < 1$, $0.2 < T < 2$ GeV. The flux-integrated CCQE total cross section, obtained by integrating the double differential cross section over this range (Table VI in Ref. [30]), was measured to be 8.447×10^{-39} cm^2 and 9.429×10^{-39} cm^2 for the range $-1 < \cos\theta < 1$, $0 < T$(GeV) $< \infty$. The total normalization error on this measurement is 10.7%. These results contain the most complete and model-independent information that is available for the CCQE process.

We calculated the flux-integrated double differential cross section $[d^2\sigma/dT\,d\cos\theta)^{\rm int}]$ for the BNB ν_μ flux within the RDWIA and RFGM models with the extracted values of M_A using the T and Q^2 bins from Ref. [30]

$$\left(\frac{d^2\sigma}{dT\,d\cos\theta}\right)_{ij}^{\rm int} = \frac{1}{\Delta T\,\Delta\cos\theta}\int_{T_i}^{T_{i+1}}\int_{(\cos\theta)_j}^{(\cos\theta)_{j+1}}\left[\frac{d^2\sigma}{dT\,d\cos\theta}(T,\cos\theta)\right]^{\rm int} \times dT\,d\cos\theta, \quad (22)$$

where $\Delta T = T_{i+1} - T_i = 0.1$ GeV and $\Delta\cos\theta = (\cos\theta)_{j+1} - (\cos\theta)_j = 0.1$.

Figures 4 and 5 show measured flux-integrated $d^2\sigma/dT\,d\cos\theta$ cross sections as functions of $\cos\theta$ for several bins of muon kinetic energy in the range $0.2 \leqslant T \leqslant 2$ GeV as compared with the RDWIA and RFGM calculations. There is good agreement between the RDWIA calculations and data within the error of the experiment. However, in the regions $0.2 \leqslant T \leqslant 0.3$ GeV, $-1 \leqslant \cos\theta \leqslant -0.3$, and $0.2 \leqslant T \leqslant 0.5$ GeV, $0.9 \leqslant \cos\theta \leqslant 1$ the RDWIA result is slightly lower than the measured cross section and the difference decreases with muon energy. The RFGM prediction also agrees well with the data, except in the regions $0.7 < \cos\theta < 1$ and $0.2 < T < 0.5$ GeV, where the calculated cross sections fall rapidly with $\cos\theta$. In this kinematic region, the Fermi gas model underestimates the double differential cross section significantly. This trend is characteristic of the nucleon momentum distribution and Pauli blocking effect as calculated in the Fermi gas model [48].

Figure 6 shows measured flux-integrated $d^2\sigma/dT\,d\cos\theta$ cross sections as functions of muon energy for four bins of the muon scattering angle compared with the RDWIA and RFGM calculations. The RDWIA cross sections are lower than the data in the kinematic region $0.9 < \cos\theta < 1$, $0.2 \leqslant T \leqslant 0.5$ (GeV) and the RFGM calculation underestimates the measured double differential cross section significantly in the range $0.7 < \cos\theta < 1$, $0.2 < T < 0.5$ GeV.

So, the comparison of measured to calculated flux-integrated $d^2\sigma/dT\,d\cos\theta$ cross sections shows that the Fermi gas model prediction are significantly lower than the data in the range $0.7 < \cos\theta < 1$, $0.2 < T < 0.5$ GeV. The RDWIA cross sections underestimate the data for muon production with energies $T \leqslant 0.3$ GeV and scattering angles $\cos\theta > 0.9$.

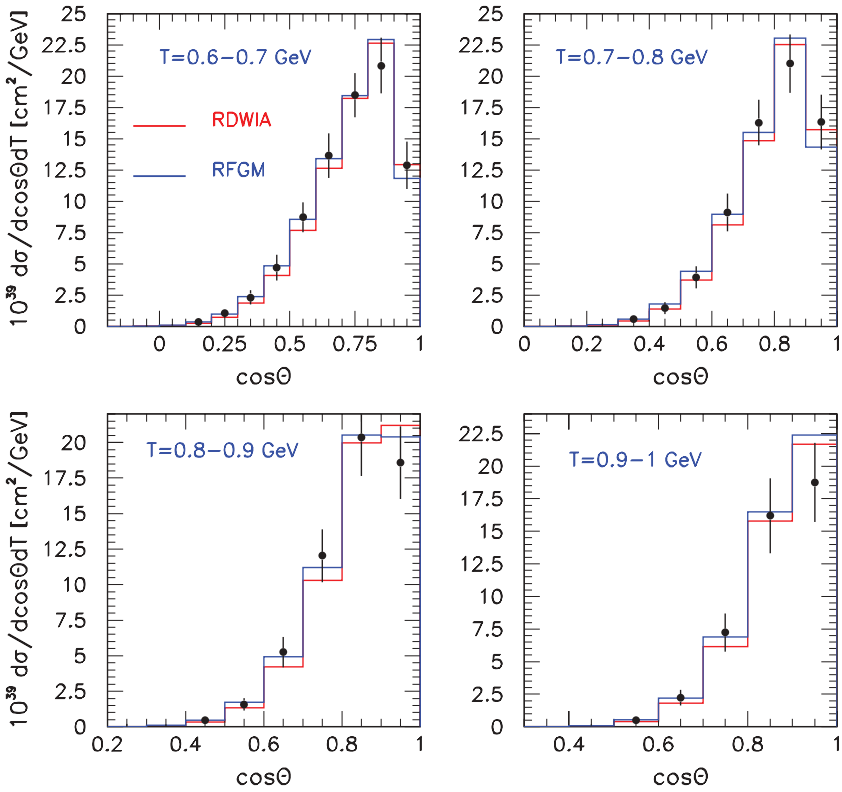

FIG. 5. (Color online) Same as Fig. 4 but for muon kinetic energy bins: T(GeV) = (0.6–0.7), (0.7–0.8), (0.8–0.9), and (0.9–1).

C. CCQE flux-integrated $d\sigma/dT$ and $d\sigma/d\cos\theta$ cross section

The flux-integrated single differential cross sections $d\sigma/dT$ and $d\sigma/d\cos\theta$ (for $T \geqslant 0.2$ GeV) are presented in Fig. 7, which shows $d\sigma/dT$ as a function of muon kinetic energy and $d\sigma/d\cos\theta$ as a function of the muon scattering angle. Here the results obtained in the RDWIA and Fermi gas models are compared with the MiniBooNE data.

The measured flux-integrated $d\sigma/dT$ ($d\sigma/d\cos\theta$) cross section with the shape error was obtained by summing the double differential cross section over $\cos\theta$ bins (T bins)

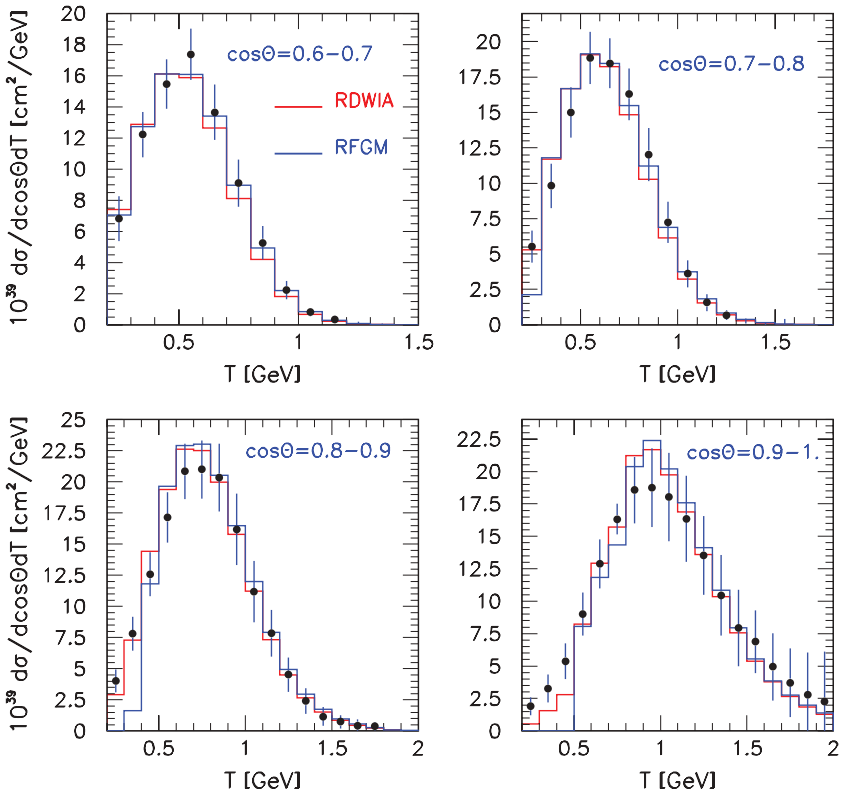

FIG. 6. (Color online) Flux-integrated $d^2\sigma/dTd\cos\theta$ per neutron cross section for the ν_μ CCQE process as a function of muon energy for the four muon scattering angle bins: $\cos\theta$ = (0.6–0.7), (0.7–0.8), (0.8–0.9), and (0.9–1). As shown in the key, cross sections were calculated within the RDWIA ($M_A = 1.37$ GeV/c^2) and RFGM ($M_A = 1.36$ GeV/c^2). The MiniBooNE data are shown as points with the shape error only.

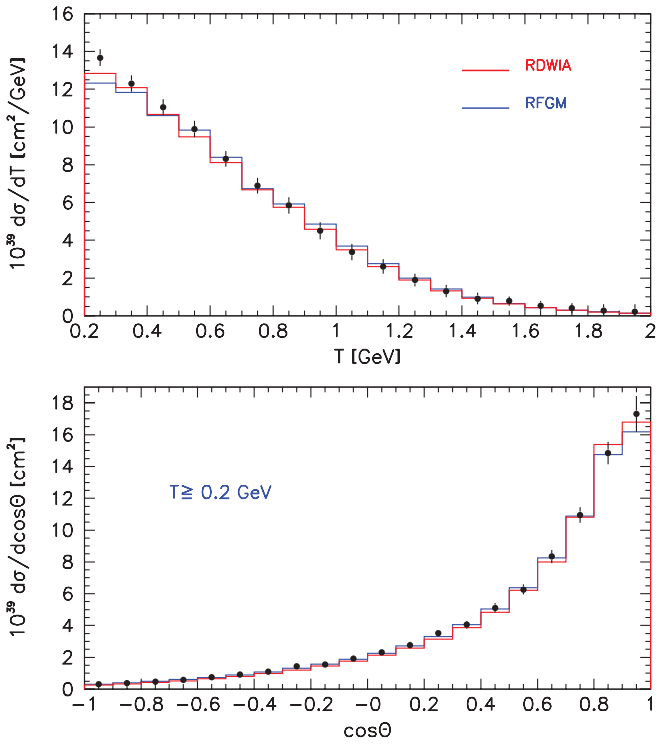

FIG. 7. (Color online) Flux-integrated $d\sigma/dT$ cross section as a function of muon energy (upper panel) and $d\sigma/d\cos\theta$ cross section for $T \geqslant 0.2$ GeV as a function of muon scattering angle (lower panel) for the ν_μ CCQE process. As shown in the key, cross sections were calculated within the RDWIA and RFGM. The MiniBooNE data are shown as points with the shape error only.

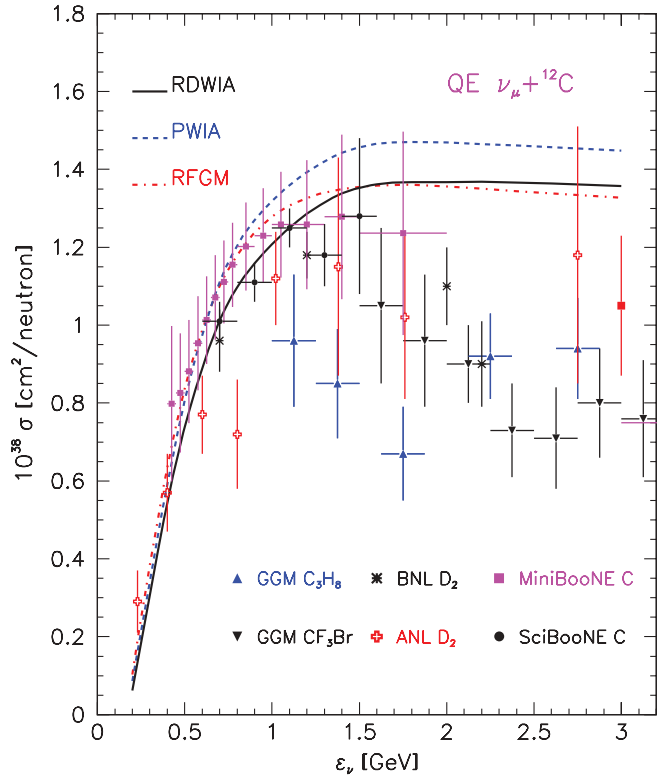

FIG. 8. (Color online) Total ν_μ CCQE per neutron cross section as a function of neutrino energy. Data points for different targets are from Refs. [25,30,49–52]. Also shown are predictions of the RDWIA ($M_A = 1.37$ GeV/c^2), PWIA ($M_A = 1.37$ GeV/c^2), and RFGM ($M_A = 1.36$ GeV/c^2).

presented in Tables VI and VII in Ref. [30]. There is good agreement between the calculated and measured cross sections, with the exception of the bin $0.2 \leqslant T \leqslant 0.3$ GeV. The flux-integrated total cross sections obtained in the RDWIA and RFGM approaches by integrating the double differential cross sections (over $-1 \leqslant \cos\theta \leqslant 1$, $0.2 \leqslant T \leqslant 2$ GeV) are equal to 8.208×10^{-39} cm^2 and 8.310×10^{-39} cm^2, correspondingly, and agree with the measured value of 8.447×10^{-39} cm^2.

D. CCQE total cross section

The MiniBooNE flux-unfolded CCQE per neutron cross section as a function of neutrino energy is shown in Fig. 8 together with the data of Refs. [49–52]. Also shown for comparison are the results obtained in the RDWIA, PWIA, and RFGM approaches. The calculated cross sections, which use the values of M_A extracted from the shape-only fit to the flux-integrated $d\sigma/Q^2$ data, reproduce the MiniBooNE total cross section within the experimental errors over the entire measured energy range. At the average energy of the MiniBooNE flux (≈800 MeV), the extracted cross section is ≈30% higher than what is commonly assumed for this process assuming the RFGM and world-average value of the axial mass $M_A = 1.03$ GeV/c^2. Note that the spread in the data is much higher than the difference in predictions of the RDWIA, PWIA, and RFGM approaches. So the comparison of the predicted and measured model-independent flux-integrated double differential cross sections is more a sensitive test of the employed models of the CCQE process than the comparison of the total cross sections.

IV. CONCLUSION

In this article, we analyzed the flux-averaged and flux-integrated differential and total ν_μ CCQE cross sections, placing particular emphasis on their nuclear-model dependence. We found that the extracted flux-integrated cross sections feature minimal model dependence. The flux-integrated double differential $d^2\sigma/dTd\cos\theta$, single differential $d\sigma/dQ^2$, $d\sigma/dT$, $d\sigma/d\cos\theta$, and flux-unfolded $\sigma(\varepsilon_i)$ CCQE cross sections were measured in the MiniBooNE experiment [30].

Using the RDWIA and RFGM approaches with the BNB flux, we extracted an axial mass from a "shape-only" fit of the measured flux-integrated $d\sigma/dQ^2$ differential cross section. The extracted values of $M_A = 1.37 \pm 0.05$ GeV/c^2 (RDWIA) and $M_A = 1.36 \pm 0.05$ GeV/c^2 (RFGM) are consistent with the MiniBooNE result of $M_A = 1.35 \pm 0.17$ GeV/c^2. The flux-integrated double differential cross sections were calculated in these models with the extracted values of M_A. There is an overall agreement between the RDWIA result and data, whereas the RFGM calculation overestimates the measured cross section at $Q^2 < 0.2$ (GeV/c)^2. Thus, the so-called

low-Q^2 problem is successfully solved in the framework of RDWIA.

We also calculated in the RDWIA and RFGM approaches the flux-integrated $d^2\sigma/dTd\cos\theta$, $d\sigma/dQ^2$, $d\sigma/dT$ (for muons with kinetic energy $T \geqslant 0.2$ GeV), and total cross sections and compared them with the MiniBooNE data. The RDWIA double differential cross section shows good agreement with the data, except in the region $0.2 \leqslant T \leqslant 0.3$ GeV, $0.9 \leqslant \cos\theta \leqslant 1$ where the calculated cross sections are lower than the measured ones. Good agreement between the RFGM calculation and data is observed exclusive of the range $0.7 \leqslant \cos\theta 1, 0.2 \leqslant T \leqslant 0.5$ GeV where the Fermi gas model predictions are completely off from the data. The calculated $d\sigma/dT$ and $d\sigma/d\cos\theta$ also describe well the measured cross sections except in the muon energy bin $0.2 \leqslant T \leqslant 0.3$ GeV where the calculations are lower than the data.

The calculated and measured flux-integrated total cross sections match well. The RDWIA, PWIA, and RFGM calculations with the extracted values of M_A reproduce the MiniBooNE flux-unfolded CCQE cross section within the experimental error over the entire measured energy range.

We conclude that the extracted flux-integrated double differential cross section should be used as the preferred choice for comparison to the employed model of the CCQE interaction on nuclear targets.

ACKNOWLEDGMENTS

The author greatly acknowledges J. Morfin, G. Zeller, T. Katori, R. Bradford, and B. Tice for fruitful discussions at different stages of this work.

[1] A. A. Aguilar-Arevalo *et al.* (MiniBooNE Collaboration), Phys. Rev. Lett. **100**, 032301 (2008).
[2] P. Adamson *et al.* (MINOS Collaboration), Phys. Rev. D **77**, 072002 (2008).
[3] A. Ferrero *et al.* (T2K Collaboration), AIP Conf. Proc. **1189**, 77 (2009).
[4] G. Rosa *et al.* (OPERA Collaboration), Nucl. Phys. B, Proc. Suppl. **145**, 98 (2005).
[5] D. S. Ayres *et al.* (NOvA Collaboration), arXiv:hep-ex/0503053.
[6] R. A. Smith and E. J. Moniz, Nucl. Phys. B **43**, 605 (1972); **101**, 547 (1975).
[7] H. Kim, J. Piekarewicz, and C. J. Horowitz, Phys. Rev. C **51**, 2739 (1995).
[8] J. Nieves, M. Valverde, and M. J. Vicente Vacas, Phys. Rev. C **73**, 025504 (2006).
[9] A. Meucci, C. Giusti, and F. D. Pacati, Nucl. Phys. A **739**, 277 (2004).
[10] C. Maieron, M. C. Martinez, J. A. Caballero, and J. M. Udias, Phys. Rev. C **68**, 048501 (2003).
[11] M. C. Martinez, P. Lava, N. Jachowicz, J. Ryckebusch, K. Vantournhout, and J. M. Udias, Phys. Rev. C **73**, 024607 (2006).
[12] O. Benhar, N. Farina, H. Nakamura, M. Sakuda, and R. Seki, Phys. Rev. D **72**, 053005 (2005).
[13] K. S. Kim, M. K. Cheoun, and B. G. Yu, Phys. Rev. C **77**, 054604 (2008).
[14] M. S. Athar, S. Chauhan, S. K. Singh, and M. J. Vicente Vacas, arXiv:0808.1437.
[15] T. Leitner, O. Buss, L. Alvarez-Ruso, and U. Mosel, Phys. Rev. C **79**, 034601 (2009).
[16] M. Martini, M. Ericson, G. Chanfray, and J. Marteau, Phys. Rev. C **80**, 065501 (2009).
[17] A. V. Butkevich and S. A. Kulagin, Phys. Rev. C **76**, 045502 (2007).
[18] A. V. Butkevich, Phys. Rev. C **80**, 014610 (2009).
[19] S. Boyd, S. Dytman, E. Hernandez, and R. Tacik, AIP Conf. Proc. **1189**, 60 (2009).
[20] K. S. Kuzmin, V. V. Lyubushkin, and V. A. Naumov, Eur. Phys. J. C **54**, 517 (2008).
[21] V. Bernard, L. E. Elouadrhiri, U.-G. Meissner, J. Phys. G **28**, R1 (2002).
[22] V. Lyubushkin *et al.* (NOMAD Collaboration), Eur. Phys. J. C **63**, 355 (2009).
[23] R. Gran *et al.* (K2K Collaboration), Phys. Rev. D **74**, 052002 (2006).
[24] X. Espinal and F. Sanchez, AIP Conf. Proc. **967**, 117 (2007).
[25] J. L. Alcaraz-Aunion and J. Walding (SciBooNE Collaboration), AIP Conf. Proc. **1189**, 145 (2009).
[26] M. Dorman *et al.* (MINOS Collaboration), AIP Conf. Proc. **1189**, 133 (2009).
[27] A. V. Butkevich and S. P. Mikheyev, Phys. Rev. C **72**, 025501 (2005).
[28] K. S. McFarland *et al.* (MiNERvA Collaboration), Nucl. Phys. B, Proc. Suppl. **159**, 107 (2006).
[29] M. Soderberg *et al.* (MicroBooNE Collaboration), AIP Conf. Proc. **1189**, 83 (2009).
[30] A. A. Aguilar-Arevalo *et al.* (MiniBooNE Collaboration), Phys. Rev. D **81**, 092005 (2010).
[31] P. Mergell, U.-G. Meissner, and D. Drechesel, Nucl. Phys. A **596**, 367 (1996).
[32] T. de Forest, Nucl. Phys. A **392**, 232 (1983).
[33] D. Dutta *et al.*, Phys. Rev. C **68**, 064603 (2003).
[34] J. J. Kelly, Phys. Rev. C **71**, 064610 (2005).
[35] B. D. Serot and J. D. Walecka, Adv. Nucl. Phys. **16**, 1 (1986).
[36] C. J. Horowitz, D. P. Murdock, and B. D. Serot, in *Computational Nuclear Physics 1: Nuclear Structure*, edited by K. Langanke, J. A. Maruhn, and S. E. Koonin (Springer-Verlag, Berlin, 1991), p. 129.
[37] D. Rohe *et al.*, Nucl. Phys. B, Proc. Suppl. **159**, 152 (2006).
[38] J. J. Kelly, Phys. Rev. C **59**, 3256 (1999).
[39] J. J Kelly, [http://www.physics.umd.edu/enp/jjkelly/LEA].
[40] E.D. Cooper, S. Hama, B. C. Clark, and R. L. Mercer, Phys. Rev. C **47**, 297 (1993).
[41] K. G. Fissum *et al.*, Phys. Rev. C **70**, 034606 (2004).
[42] A. Meucci, F. Capuzzi, C. Giusti, and F. D. Pacati, Phys. Rev. C **67**, 054601 (2003).
[43] A. Meucci, C. Giusti, and F. D. Pacati, Nucl. Phys. A **744**, 307 (2004).
[44] S. A. Kulagin and R. Petti, Nucl. Phys. A **765**, 126 (2006).

[45] C. Ciofi degli Atti and S. Simula, Phys. Rev. C **53**, 1689 (1996).
[46] A. A. Aguilar-Arevalo *et al.* (MiniBooNE Collaboration), Phys. Rev. D **79**, 072002 (2009).
[47] T. Katori *et al.* (MiniBooNE Collaboration), AIP Conf. Proc. **1189**, 139 (2009).
[48] A. V. Butkevich, Phys. Rev. C **78**, 015501 (2008).
[49] W. A. Mann *et al.*, Phys. Rev. Lett. **31**, 844 (1973).
[50] N. J. Baker *et al.*, Phys. Rev. D **23**, 2499 (1981).
[51] M. Pohl *et al.*, Lett. Nuovo Cimento **26**, 332 1979.
[52] J. Brunner *et al.*, Z. Phys. C **45**, 551 (1990).